Derivation of the Fano profile from time-dependent density-functional theory for local thermodynamic equilibrium plasmas

Shuji Kiyokawa
Department of Physics, Faculty of Science, Nara Women's University, Kitauoyanishi-Machi, Nara 630-8506, Japan
(Received 19 October 2006; revised manuscript received 9 January 2007; published 3 April 2007)

We give the derivation of the Fano profile (the resonance energy position, the resonance width Γ, and q value) from the time-dependent nonrelativistic density-functional theory (DFT) and propose a scheme for calculating the photoabsorption cross section of hot dense plasmas. As a consequence of this derivation, we show the line profile is obtained as a superposition of Fano and Lorentz profiles when the competition of two optically allowed bound-bound and bound-free transitions occurs. We also show the results of the photoabsorption cross section by applying our scheme to an Fe plasma (density is 7.85 g/cm^3, temperature is 100 eV), where the calculation is carried out without numerical divergence for any photon energy. The calculated results are in good agreement with those of Grimaldi.

DOI: 10.1103/PhysRevA.75.042501 PACS number(s): 32.70.−n, 32.90.+a, 52.25.Os, 52.27.Gr

I. INTRODUCTION

In hot dense plasmas such as inertial confinement plasmas and the interior of stars, the thermal properties (such as ion-ion correlation, the charge state distribution, and so on) and the atomic ones (such as the spectral properties, electronic states, the level occupation number of electron, and so on) are closely correlated with each other. The former have been sufficiently investigated theoretically and experimentally by many authors. The latter, namely, the numerical data on the atom or ion in the plasmas, are becoming available in recent years.

The average atom (AA) model [1–4] and the finite temperature density-functional theory (FTDFT) [5,6] have been employed vigorously to study the equation of state (EOS) [7–10] photoabsorption [11,12], opacity [13], and so on for the local thermodynamic equilibrium (LTE) plasmas. As an actual LTE plasma is composed of various ions in different excited states and charge states, the spectral structure of LTE plasma is very complex because of the enormous number of transition lines. The method of the supertransition array (STA) [9,13–15] has been used to analyse the complex line spectrum of an ion in a LTE plasma, where the ionic charge state distribution of the plasma is drawn from the AA which has noninteger occupation numbers of electrons.

For the photoabsorption of an isolated atom by time-dependent DFT (TDDFT), it has been established that the relaxation of the electronic system under the radiation field is very important [16–18]. The photoabsorption cross section for an isolated atom calculated with the relaxation is in good agreement with experiments [19–23]. In the case of the LTE plasmas, Grimaldi *et al.* [24] applied TDDFT to the photoabsorption of the dense Fe plasmas and showed that relaxation of the electronic system drastically changes the photoabsorption cross section. They also examined the plasma level broadening and the self-energy effect, but they did not consider the accurate ion-ion pair distribution function in the calculation.

There are some problems, however, with the TDDFT proposed by Zangwill and Soven (ZS theory) [16] which is applied to the calculation of photoabsorption:

(i) The calculation does not give the correct resonance energy position for photoabsorption due to the local density approximation employed for the exchange-correlation potential.

(ii) For photon energies in the vicinity of a peak of Fano profile, one encounters a numerical difficulty in calculating the photoabsorption cross section with the theory, that is, in most cases, a long computation time is required to obtain convergence, and sometimes the calculation does not converge. One way to avoid this numerical difficulty is to use a fitting method for the resonance line shape, following [25], which uses fitting parameters such as resonance energy position, resonance width Γ, and the q value for the Fano profile.

The purpose of this paper is to give a derivation of the Fano profile from the nonrelativistic TDDFT and to propose a scheme for calculating the photoabsorption cross section of plasmas without the numerical difficulty pointed out in (ii) above. In this scheme, the resonance energy position of the photoabsorption obtained does not equal the difference of the eigenvalues of the Kohn-Sham equation with the local density approximation (hereafter LDA) which are related to the optically allowed transitions, but includes a shift to a more accurate energy. Therefore, our scheme also solves the above problem (i) approximately, but without the effect of the nearest-neighbor interaction on the photoabsorption [26]. Moreover, it is shown from this derivation that the line profile is expressed by a superposition of the Fano and the Lorentz profiles in the case where competition of two optically allowed bound-bound and bound-free transitions occurs.

In Sec. II, we first describe our nonrelativistic FTDFT of the plasma [27] which gives the wave functions and eigenvalues used to obtain the best one-electron density of the AA in a plasma. In our FTDFT, the ion distribution [the ion-ion pair correlation function $g_{ii}(r)$] is calculated using the hypernetted-chain (HNC) equation. Then, we present the scheme for calculating the photoabsorption cross section of the plasma. We also give a derivation of the Fano profile (resonance energy position, resonance width Γ, and q value)

with the TDDFT. In Sec. III, we show the numerical results of the photoabsorption cross section for a dense Fe plasma obtained by use of our scheme, and compare it with those of Grimaldi [24]. The concluding remarks are given in Sec. IV.

II. DESCRIPTION OF THE SCHEME

Here, we consider a charge-neutral plasma in LTE whose ion number density is ρ_{ion} and temperature is T in energy units. We assume the plasma consist of average atoms whose nuclear charge is $+Ze$ and a uniform background electron density.

A. Finite temperature DFT of plasmas

There has been addressed many useful theories for the studying of thermal properties or electronic structure of hot dense plasmas [5,6,28,29], however, we briefly show our nonrelativistic FTDFT of the hot dense plasmas [8,27]. Our theory assumes the plasma is composed of the average atom allowed to have noninteger occupation number of bound electrons and uniform background electrons in continuum states. Though the electronic structure of plasmas is very complex because of resonances from the continuum density of states [30,31], our FTDFT treats the continuum states as plane waves instead of wave functions obtained from the LDA equation.

The possible bound state wave functions of the average atom are obtained by solving the following LDA equation (hereafter, we use atomic units):

$$\left(-\frac{1}{2}\nabla^2 + V(r)\right)\psi_{n\ell}(\boldsymbol{r}) = \varepsilon_{n\ell}\psi_{n\ell}(\boldsymbol{r}), \tag{1}$$

where the potential $V(r)$ for the AA is given as

$$V(r) = -\frac{Z}{r} + \int \frac{\rho_b(\boldsymbol{r}')}{|\boldsymbol{r}-\boldsymbol{r}'|}d\boldsymbol{r}' - \int \frac{Q_s(\boldsymbol{r}')}{|\boldsymbol{r}-\boldsymbol{r}'|}d\boldsymbol{r}' + v_{xc}[\rho_b(\boldsymbol{r}) + \rho_c] - v_{xc}[\rho_c]. \tag{2}$$

The $\rho_b(\boldsymbol{r})$ is the density of the bound electrons in the AA,

$$\rho_b(\boldsymbol{r}) = 2\sum_{n\ell} f(\varepsilon_{n\ell})|\psi_{n\ell}(\boldsymbol{r})|^2, \tag{3}$$

where the factor $f(\varepsilon_{n\ell})$ is the Fermi distribution function,

$$f(\varepsilon) = \frac{1}{e^{\beta(\varepsilon-\mu)}+1}. \tag{4}$$

The fourth and the fifth terms on the right-hand side of Eq. (2), $v_{xc}[\rho]$, are the exchange-correlation potentials in the case of finite temperature [32]. The form of the exchange-correlation potential employed here is given in Appendix B of the present paper.

The boundary condition for the wave function is given by

$$\psi_{n\ell}(\boldsymbol{r}) \sim 0, \quad |\boldsymbol{r}| \to \infty. \tag{5}$$

This means that the bound electrons in the AA are not confined in the ion sphere, where the ion-sphere radius a_{ion} is defined as $\frac{4\pi}{3}a_{ion}^3\rho_{ion}=1$.

The chemical potential μ in Eq. (4) is obtained from the conservation of the number of electrons per an AA,

$$Z = 2\sum_{n\ell} f(\varepsilon_{n\ell}) + Z^*, \tag{6}$$

where Z^* is the noninteger charge of the AA, which is defined by Eq. (8) below.

The function $Q_s(\boldsymbol{r})$ in the third term on the right-hand side of Eq. (2) is the charge density, composed of three parts: the charge densities of the nucleus, the bound electrons of the other average atoms surrounding the AA located at the origin of the coordinate system, and the uniform background electron charge density $-\rho_c$,

$$Q_s(\boldsymbol{r}) = Z\rho_{ion}g_{ii}(\boldsymbol{r}) - \rho_{ion}\int \rho_b(\boldsymbol{r}-\boldsymbol{R})g_{ii}(\boldsymbol{R})d\boldsymbol{R} - \rho_c. \tag{7}$$

The ρ_c in Eq. (7) is given as

$$\rho_c = Z^*\rho_{ion} = \frac{1}{\pi^2}\int \frac{\sqrt{2\varepsilon}}{e^{\beta(\varepsilon-\mu)}+1}d\varepsilon. \tag{8}$$

The function $g_{ii}(\boldsymbol{r})$ on the right-hand side of Eq. (7) is the pair distribution function of ions in the plasma, and it is calculated by HNC approximation as

$$G_{ii}(\boldsymbol{r}) = C(\boldsymbol{r}) + \rho_{ion}\int C(\boldsymbol{r}-\boldsymbol{r}')G_{ii}(\boldsymbol{r}')d\boldsymbol{r}', \tag{9}$$

$$N(\boldsymbol{r}) = \rho_{ion}\int C(\boldsymbol{r}-\boldsymbol{r}')G_{ii}(\boldsymbol{r}')d\boldsymbol{r}', \tag{10}$$

$$g_{ii}(r) = e^{N(r)-\beta\phi(r)}, \tag{11}$$

where $G_{ii}(\boldsymbol{r})=g_{ii}(r)-1$. Equation (9) is called the Ornstein-Zernike's relation, and defines the direct correlation function $C(\boldsymbol{r})$. The Fourier transform $\tilde{\phi}(\boldsymbol{k})$ of the interatomic interaction $\phi(r)$ in Eq. (11) is given as

$$\tilde{\phi}(\boldsymbol{k}) = \frac{4\pi}{k^2}[Z - \tilde{\rho}_b(\boldsymbol{k})]^2, \tag{12}$$

where $\tilde{\rho}_b(\boldsymbol{k})$ is the Fourier transform of the bound electron density $\rho_b(\boldsymbol{r})$ of Eq. (3). For simplicity, our FTDFT does not include the effect of the polarization of continuum electrons on the ion-ion interaction.

B. Derivation of Fano profile

We now discuss the photoresponse of an AA in plasmas to a frequency-dependent external field. If the incident photon energy $\hbar\omega$ is in the vicinity of the difference between two orbital energies $\varepsilon_{n_i\ell_i}$ and $\varepsilon_{n_f\ell_f}(|\ell_i-\ell_f|=1)$, i.e., $\hbar\omega\sim\varepsilon_{n_f\ell_f}-\varepsilon_{n_i\ell_i}$ with $\varepsilon_{n_f\ell_f}-\varepsilon_{n_i\ell_i}>|\varepsilon_{n_f\ell_f}|$, one of the $(n_f\ell_f)$ electrons can attain an energy above the ionization energy via the following successive excitation processes:

$$(n_i\ell_i)^a(n_f\ell_f)^b \to (n_i\ell_i)^{a-1}(n_f\ell_f)^{b+1} \to (n_i\ell_i)^a(n_f\ell_f)^{b-1}(\varepsilon\,\ell\,),$$

consequently, the $(n_f\ell_f)$ electron can be ejected. Another process can coincide with this process, that is, one of the $(n_f\ell_f)$

electrons can directly absorb the photon energy $\hbar\omega$:

$$(n_i\ell_i)^a(n_f\ell_f)^b \rightarrow (n_i\ell_i)^a(n_f\ell_f)^{b-1}(\varepsilon\,\ell\,).$$

These two processes compete with each other, namely, a channel mixing occurs, and consequently, the Fano profile appears on the photoabsorption cross section. If the energies of the $\varepsilon_{n_i\ell_i}$ and the $\varepsilon_{n_f\ell_f}$ do not satisfy the condition $\varepsilon_{n_f\ell_f}-\varepsilon_{n_i\ell_i}>|\varepsilon_{n_f\ell_f}|$, the channel mixing cannot occur in our calculation, but a direct bound-bound transition $(n_i\ell_i)^a(n_f\ell_f)^b \rightarrow (n_i\ell_i)^{a-1}(n_f\ell_f)^{b+1}$ can occur if the photon energy satisfies the resonance condition $\hbar\omega=\varepsilon_{n_f\ell_f}-\varepsilon_{n_i\ell_i}$. To investigate the above processes, we study how the electrons respond to a frequency-dependent external field.

1. Formulation of the photoabsorption

We assume that the frequency dependent external electric field is of magnitude E_0 directed along the z axis. The interaction between this field and the electrons of the AA is $\int\rho(\boldsymbol{r})\phi_{ext}(\boldsymbol{r},\omega)e^{i\omega t}d\boldsymbol{r}$, where $\rho(\boldsymbol{r})$ is the electron density and

$$\phi_{ext}(\boldsymbol{r},\omega)=E_0 z. \tag{13}$$

The induced charge density $\delta\rho(\boldsymbol{r},\omega)$ in the presence of the external field $\phi_{ext}(\boldsymbol{r},\omega)$ is calculated by means of the single particle response function $\chi^0(\boldsymbol{r},\boldsymbol{r}';\omega)$ [24] as follows:

$$\delta\rho(\boldsymbol{r},\omega)=\int \chi^0(\boldsymbol{r},\boldsymbol{r}';\omega)\phi_{scf}(\boldsymbol{r},\omega)d\boldsymbol{r}, \tag{14}$$

where $\phi_{scf}(\boldsymbol{r},\omega)$ is the self-consistent field produced by the photoresponse of the electrons. The self-consistent field $\phi_{scf}(\boldsymbol{r},\omega)$ is determined by the following relations:

$$\phi_{scf}(\boldsymbol{r},\omega)=\phi_{ext}(\boldsymbol{r},\omega)+\phi_{ind}(\boldsymbol{r},\omega), \tag{15}$$

$$\phi_{ind}(\boldsymbol{r},\omega)=\int K(\boldsymbol{r},\boldsymbol{r}')\delta\rho(\boldsymbol{r},\omega)d\boldsymbol{r}', \tag{16}$$

$$K(\boldsymbol{r},\boldsymbol{r}')=\frac{1}{|\boldsymbol{r}-\boldsymbol{r}'|}+\left.\frac{\delta v_{xc}[\rho]}{\delta\rho}\right|_{\rho=\rho(r)}\delta(\boldsymbol{r}-\boldsymbol{r}'), \tag{17}$$

where $\phi_{ind}(\boldsymbol{r},\omega)$ is the frequency-dependent-induced potential. The kernel function $K(\boldsymbol{r},\boldsymbol{r}')$ is assumed to be static [16,24].

The response function $\chi^0(\boldsymbol{r},\boldsymbol{r}';\omega)$ in Eq. (14) is given as

$$\chi^0(\boldsymbol{r},\boldsymbol{r}';\omega)=2\sum_{ij}[f(\varepsilon_i)-f(\varepsilon_j)]\frac{\psi_i^*(\boldsymbol{r})\psi_j(\boldsymbol{r})\psi_j^*(\boldsymbol{r}')\psi_i(\boldsymbol{r}')}{\omega-(\varepsilon_j-\varepsilon_i)+i\delta}, \tag{18}$$

where $\psi_i(\boldsymbol{r})$ and ε_i are the wave functions and eigenvalues obtained from the LDA equation, Eq. (1), and the sum is supposed to be over all bound and continuum states. The factor 2 on the right-hand side of Eq. (18) comes from the sum with respect to the electron spin.

We first separate the radial and the angular parts of $\phi_{ext}(\boldsymbol{r},\omega)$, $\phi_{scf}(\boldsymbol{r},\omega)$, $\delta\rho(\boldsymbol{r},\omega)$, and $\chi^0(\boldsymbol{r},\boldsymbol{r}';\omega)$ as follows:

$$\phi_{ext}(\boldsymbol{r},\omega)=E_0\sqrt{\frac{4\pi}{3}}rY_{10}(\hat{\boldsymbol{r}}), \tag{19}$$

$$\phi_{scf}(\boldsymbol{r},\omega)=E_0\phi_\omega^{scf}(r)Y_{10}(\hat{\boldsymbol{r}}), \tag{20}$$

$$\delta\rho(\boldsymbol{r},\omega)=E_0\delta\rho_\omega(r)Y_{10}(\hat{\boldsymbol{r}}), \tag{21}$$

$$\chi^0(\boldsymbol{r},\boldsymbol{r}';\omega)=\sum_{\ell m}Y_{\ell m}^*(\hat{\boldsymbol{r}})\chi_\omega^0(r,r')Y_{\ell m}(\hat{\boldsymbol{r}}'), \tag{22}$$

where $Y_{\ell m}(\hat{\boldsymbol{r}})$ is the spherical harmonic.

Substituting $\psi(\boldsymbol{r})=R_{n\ell}(r)Y_{\ell m}(\hat{\boldsymbol{r}})$ [$R_{n\ell}(r)$ is the radial wave function] into Eq. (18), we obtain the radial part of the single particle response function $\chi_\omega^0(r,r')$ [17],

$$\begin{aligned}\chi_\omega^0(r,r')=&\sum_{n\ell}\sum_{n'\ell'}2[f(\varepsilon_{n\ell})-f(\varepsilon_{n'\ell'})]C_{\ell\ell'}\frac{R_{n\ell}(r)R_{n'\ell'}(r)R_{n'\ell'}(r')R_{n\ell}(r')}{\varepsilon_{n\ell}-\varepsilon_{n'\ell'}+\omega+i\delta}+\sum_{n\ell\ell'}\int 2[f(\varepsilon_{n\ell})-f(\varepsilon)]C_{\ell\ell'}\\&\times\frac{R_{n\ell}(r)R_{\varepsilon\ell'}(r)R_{\varepsilon\ell'}(r')R_{n\ell}(r')}{\varepsilon_{n\ell}-\varepsilon+\omega+i\delta}d\varepsilon+\sum_{n\ell\ell'}\int 2[f(\varepsilon)-f(\varepsilon_{n\ell})]C_{\ell\ell'}\frac{R_{\varepsilon\ell'}(r)R_{n\ell}(r)R_{n\ell}(r')R_{\varepsilon\ell'}(r')}{\varepsilon-\varepsilon_{n\ell}+\omega+i\delta}d\varepsilon\\&+\sum_{\ell\ell'}\int\int 2[f(\varepsilon)-f(\varepsilon')]C_{\ell\ell'}\frac{R_{\varepsilon\ell}(r)R_{\varepsilon'\ell'}(r)R_{\varepsilon'\ell'}(r')R_{\varepsilon\ell}(r')}{\varepsilon-\varepsilon'+\omega+i\delta}d\varepsilon d\varepsilon'.\end{aligned} \tag{23}$$

The factor $C_{\ell\ell'}$ in Eq. (23) is given by

$$C_{\ell\ell'}=\frac{1}{4\pi}(2\,\ell\,+1)(2\ell'+1)\begin{pmatrix}\ell & \ell' & 1\\ 0 & 0 & 0\end{pmatrix}^2, \tag{24}$$

where the 2×3 matrix is a $3-j$ symbol.

The $R_{\varepsilon\ell}(r)$ in Eq. (23) is the radial wave function of a electron of energy ε and angular momentum ℓ, which is obtained by solving Eq. (1), namely,

$$\frac{1}{r^2}\frac{d}{dr}\left(r^2\frac{dR_{\varepsilon\ell}(r)}{dr}\right)+2\left(\varepsilon-V(r)-\frac{\ell(\ell+1)}{2r^2}\right)R_{\varepsilon\ell}(r)=0. \tag{25}$$

The radial wave function $R_{\varepsilon\ell}(r)$ has an asymptotic form

$$R_{\varepsilon\ell}(r) \sim \sqrt{\frac{2}{\pi k}}\frac{1}{r}\sin\left(kr - \frac{\ell\pi}{2} + \delta_\ell\right), \quad r \to \infty, \quad (26)$$

where k is wave number, $\varepsilon = \frac{k^2}{2}$, and δ_ℓ is the phase shift. In our FTDFT, the nuclear charge of AA is screened by electrons in the plasma, therefore the potential $V(r)$ for AA in the outer region does not include a Coulomb potential proportional to $-\frac{c}{r}$. Thus a logarithmic term $-\frac{C}{k}\log(2kr)$ does not appear in the argument of the sine on the right-hand side of Eq. (26).

The photoabsorption cross section is calculated as follows [16,24],

$$\sigma(\omega) = -4\pi\alpha\omega \int\int \phi_\omega^{scf*}(r') \times [\mathrm{Im}\,\chi_\omega^0(r,r')]\phi_\omega^{scf}(r) r'^2 r^2 dr' dr, \quad (27)$$

where α is the fine-structure constant.

2. Approximation for the response function

The real part of $\chi_\omega^0(r,r')$ is not included directly in the form of the photoabsorption cross section given by Eq. (27), but the self-consistent field $\phi_\omega^{scf}(r)$ is slightly affected by this real part. Then, the principal part of the photoabsorption cross section is carried through the imaginary part of $\chi_\omega^0(r,r')$. So, it seems that the contribution to the absorption cross section from the real part of the second term on the right-hand size of Eq. (23) is small. Therefore, the second term in Eq. (23) is approximated as

$$\begin{aligned}
&\sum_{n\ell\ell'} \int 2[f(\varepsilon_{n\ell}) - f(\varepsilon)] C_{\ell\ell'} \frac{R_{n\ell}(r) R_{\varepsilon\ell'}(r) R_{\varepsilon\ell'}(r') R_{n\ell}(r')}{\varepsilon_{n\ell} - \varepsilon + \omega + i\delta} d\varepsilon \\
&= \sum_{n\ell\ell'} \int 2[f(\varepsilon_{n\ell}) - f(\varepsilon)] C_{\ell\ell'} R_{n\ell}(r) R_{\varepsilon\ell'}(r) R_{\varepsilon\ell'}(r') R_{n\ell}(r') P\frac{1}{\varepsilon_{n\ell} - \varepsilon + \omega} d\varepsilon \\
&\quad - i\pi \sum_{n\ell\ell'} 2[f(\varepsilon_{n\ell}) - f(E_f)] C_{\ell\ell'} R_{n\ell}(r) R_{E_f\ell'}(r) R_{E_f\ell'}(r') R_{n\ell}(r')\,\theta(E_f) \\
&\quad \sim - i\pi \sum_{n\ell\ell'} 2[f(\varepsilon_{n\ell}) - f(E_f)] C_{\ell\ell'} R_{n\ell}(r) R_{E_f\ell'}(r) R_{E_f\ell'}(r') R_{n\ell}(r')\,\theta(E_f), \quad (28)
\end{aligned}$$

where $E_f = \varepsilon_{n\ell} + \omega$ and $\theta(E_f)$ is the unit step function.

The third term, which is positive quantity, is also negligible in this context. At this stage, we also neglect the fourth term on the right-hand side of Eq. (23) [33].

Neglecting the real part of the second term, the third and the fourth terms on the right-hand side of Eq. (23), we obtain the approximate single-particle density response function:

$$\begin{aligned}
\chi_\omega^0(r,r') \simeq\ & 2[f(\varepsilon_{n_i\ell_i}) - f(\varepsilon_{n_f\ell_f})] C_{\ell_i\ell_f} \eta_{n_i\ell_i,n_f\ell_f} R_{n_i\ell_i}(r) R_{n_f\ell_f}(r) R_{n_f\ell_f}(r') R_{n_i\ell_i}(r') \\
&+ \sum_{\varepsilon_{n\ell} < \varepsilon_{n'\ell'}} 2[f(\varepsilon_{n\ell}) - f(\varepsilon_{n'\ell'})] C_{\ell\ell'} \eta_{n\ell,n'\ell'} R_{n\ell}(r) R_{n'\ell'}(r) R_{n'\ell'}(r') R_{n\ell}(r') \\
&- i\pi \sum_{n\ell\ell'} 2[f(\varepsilon_{n\ell}) - f(E_f)] C_{\ell\ell'} R_{n\ell}(r) R_{E_f\ell'}(r) R_{E_f\ell'}(r') R_{n\ell}(r')\,\theta(E_f), \quad (29)
\end{aligned}$$

where $\eta_{n\ell,n'\ell'}$ is given as

$$\eta_{n\ell,n'\ell'} = \frac{1}{\varepsilon_{n\ell} - \varepsilon_{n'\ell'} + \omega + i\delta} - \frac{1}{\varepsilon_{n'\ell'} - \varepsilon_{n\ell} + \omega + i\delta}. \quad (30)$$

In the second term on the right-hand side of Eq. (29), the double sum runs over all bound states on the condition $\varepsilon_{n\ell} < \varepsilon_{n'\ell'}$, but without two bound states $(n_i\ell_i)$ and $(n_f\ell_f)$, and the term of this sum vanishes unless $|\ell - \ell'| = 1$. A Fermi distribution function $f(E_f)$ appears in Eq. (29) by reason of that an ion in plasma is not isolated, so that, in the case of finite temperature, the continuum states of electrons are partially occupied.

3. The photoabsorption cross section and Fano profile

We rewrite the first term and the sum on the second term of Eq. (29) to a single sum as follows,

$$\sum_{k=0,1,2,\ldots}^{k_{max}} c_k \eta_k U_k(r) U_k(r'), \tag{31}$$

where the term of $k=0$ in above sum corresponds to the first term of Eq. (29), and the factors c_0, η_0 and the function $U_0(r)$ are given as

$$\begin{cases} c_0 = 2[f(\varepsilon_{n_i\ell_i}) - f(\varepsilon_{n_f\ell_f})]C_{\ell_i\ell_f}, \\ \eta_0 = \eta_{n_i\ell_i,n_f\ell_f}, \\ U_0(r) = R_{n_i\ell_i}(r)R_{n_f\ell_f}(r). \end{cases} \tag{32}$$

The other terms ($k=1,2,\ldots$) in the sum equation (31) correspond to the nonvanishing terms on the second term of Eq. (29), and the factors c_k, η_k and the function $U_k(r)$ are determined by a combination of two bound states as following:

$$\begin{cases} c_k = 2[f(\varepsilon_{n\ell}) - f(\varepsilon_{n'\ell'})]C_{\ell\ell'}, \\ \eta_k = \eta_{n\ell,n'\ell'}, \\ U_k(r) = R_{n\ell}(r)R_{n'\ell'}(r). \end{cases} \tag{33}$$

Here, we assume that the number of all nonvanishing terms is k_{max}. (One may refer to Appendix A, as an example.)

In similar manner, numbering $k_{max}+1$, $k_{max}+2,\ldots$ for all nonvanishing terms on the third term of Eq. (29), we rewrite it as

$$\sum_{k>k_{max}} c_k \eta_k U_k(r) U_k(r'), \tag{34}$$

where the factors c_k, η_k and the function $U_k(r)$ are, respectively,

$$\begin{cases} c_k = 2[f(\varepsilon_{n\ell}) - f(E_f)]C_{\ell\ell'}\theta(E_f), \\ \eta_k = -i\pi, \\ U_k(r) = R_{n\ell}(r)R_{E_f\ell'}(r). \end{cases} \tag{35}$$

Then, Eq. (29) can be expressed as

$$\chi^0_\omega(r,r') = \sum_{k=0}^{k_{max}} c_k \eta_k U_k(r) U_k(r') + \sum_{k>k_{max}} c_k \eta_k U_k(r) U_k(r'). \tag{36}$$

Substituting Eq. (36) into Eq. (14), we obtain the radial part of the induced electron density $\delta\rho_\omega(r)$ in Eq. (21),

$$\delta\rho_\omega(r) = c_0 U_0(r) a_0 + \sum_{k=1} c_k \eta_k U_k(r) a_k, \tag{37}$$

where complex coefficients a_0 and a_k, are given as

$$\begin{cases} a_0 = \eta_0 \int_0^\infty U_0(r)\phi^{scf}_\omega(r) r^2 dr, \\ a_k = \int_0^\infty U_k(r)\phi^{scf}_\omega(r) r^2 dr, \quad k > 0. \end{cases} \tag{38}$$

From Eqs. (15), (16), and (37), the radial part $\phi^{scf}_\omega(r)$ in Eq. (21) satisfies

$$\begin{aligned} \phi^{scf}_\omega(r) &= \phi^{ext}_\omega(r) + \int_0^\infty K(r,r')\delta\rho_\omega(r') r'^2 dr' \\ &= \phi^{ext}_\omega(r) + c_0 B_0(r) a_0 + \sum_{k=1} c_k \eta_k B_k(r) a_k, \end{aligned} \tag{39}$$

where $\phi^{ext}_\omega(r) = \sqrt{(4\pi/3)}r$ is the radial part of the external field $\phi_{ext}(\boldsymbol{r},\omega)$.

The kernel function $K(r,r')$ in the above equation is the radial part of the $K(\boldsymbol{r},\boldsymbol{r}')$ of Eq. (17):

$$K(r,r') = \frac{4\pi}{\max(r,r')} + \left.\frac{\delta V_{xc}[\rho]}{\delta\rho}\right|_{\rho=\rho(r)} \frac{\delta(r-r')}{r'^2}, \tag{40}$$

and the function $B_k(r)$ is given by

$$B_k(r) = \int_0^\infty K(r,r') U_k(r') r'^2 dr'. \tag{41}$$

The self-consistent field $\phi^{scf}_\omega(r)$ is obtained by simultaneously solving Eq. (37) and Eq. (39). Substituting Eq. (39) into Eq. (38), we obtain the relation

$$\hat{V}\begin{pmatrix} a_0 \\ a_1 \\ a_2 \\ \vdots \end{pmatrix} = \begin{pmatrix} d_0 \\ d_1 \\ d_2 \\ \vdots \end{pmatrix}, \tag{42}$$

where the factor d_k is

$$d_k = \int_0^\infty U_k(r)\phi^{ext}_\omega(r) r^2 dr, \tag{43}$$

and $\hat{V}$ is the matrix given as

$$\begin{pmatrix} 1/\eta_0 - V_{00} & -\eta_1 V_{01} & -\eta_2 V_{02} & \cdots \\ -V_{10} & 1-\eta_1 V_{11} & -\eta_2 V_{12} & \cdots \\ -V_{20} & -\eta_1 V_{21} & 1-\eta_2 V_{22} & \cdots \\ \vdots & \vdots & \vdots & \ddots \end{pmatrix}. \tag{44}$$

The factor $V_{kk'}$ in above matrix elements is given as

$$V_{kk'} = c_{k'} \int_0^\infty U_k(r) B_{k'}(r) r^2 dr. \tag{45}$$

The determinant D of the matrix $\hat{V}$ can be expanded in terms of its cofactors as follows,

$$D = \left(\frac{1}{\eta_0} - V_{00}\right)A + B, \tag{46}$$

where A and B are the determinants obtained from the cofactors of D. When the infinitesimal positive quantity δ in η_0 goes to 0, $|D|^2$ becomes

$$|D|^2 = |A|^2 \lambda^2 (e^2+1). \tag{47}$$

Here $\lambda = \mathrm{Im}(B/A)$ and e is the dimensionless reduced energy given by

$$e = \frac{\omega - \varepsilon_r}{\tilde{\Gamma}/2}. \tag{48}$$

The factor ε_r in Eq. (48) is considered as a resonance energy position of the Fano profile, and it is given by

$$\varepsilon_r = \sqrt{\Delta\varepsilon^2 + 2\Delta\varepsilon(V_{00} - \gamma)}, \tag{49}$$

where $\gamma = \mathrm{Re}(B/A)$, and $\Delta\varepsilon = \varepsilon_{n_f\ell_f} - \varepsilon_{n_i\ell_i}$ is the transition energy. The factor $\tilde{\Gamma}$ in Eq. (48) is given by

$$\tilde{\Gamma} = \frac{4\Delta\varepsilon\lambda}{\omega + \varepsilon_r}, \tag{50}$$

and it slightly depends on the photon energy. At $\varepsilon = \varepsilon_r$, however, it is possible to consider $\tilde{\Gamma}$ as the resonance width Γ of the Fano profile.

The complex coefficients a_0 and a_k satisfy the following relations the same as Eq. (46):

$$Da_0 = \left(\frac{1}{\eta_0} - V_{00}\right)A + B', \tag{51}$$

$$Da_k = \left(\frac{1}{\eta_0} - V_{00}\right)P_k + Q_k. \tag{52}$$

Therefore, we obtain the following relation for a_k:

$$|a_k|^2 = \frac{(\mathrm{Re}\, P_k)^2}{|A|^2}\frac{(e + q_{1k})^2}{(e^2 + 1)} + \frac{(\mathrm{Im}\, P_k)^2}{|A|^2}\frac{(e + q_{2k})^2}{(e^2 + 1)}, \tag{53}$$

where the factors q_{1k} and q_{2k} are

$$q_{1k} = \frac{1}{\lambda}\left(\frac{\mathrm{Re}\, Q_k}{\mathrm{Re}\, P_k} - \gamma\right), \quad q_{2k} = \frac{1}{\lambda}\left(\frac{\mathrm{Im}\, Q_k}{\mathrm{Im}\, P_k} - \gamma\right). \tag{54}$$

The right-hand side of Eq. (53) has two Fano profiles, where q_{1k} and q_{2k} are considered as the q values of those Fano profiles. As shown later, we can rewrite these two Fano profiles to a Fano profile and a Lorentz profile.

The photoabsorption cross section, Eq. (27), is rewritten with the use of a_0 and a_k as

$$\sigma(\omega) = 4\pi\alpha\omega\left[c_0\left(\mathrm{Im}\,\frac{1}{\eta_0}\right)|a_0|^2 + \sum_{k=1} c_k(-\mathrm{Im}\,\eta_k)|a_k|^2\right]. \tag{55}$$

For $\delta \to 0$, we obtain

$$\mathrm{Im}\left(\frac{1}{\eta_0}\right) = \delta\frac{\omega}{\Delta\varepsilon} \to 0 (\delta \to 0), \tag{56}$$

$$\lim_{\delta\to 0}(-\mathrm{Im}\,\eta_k) = \begin{cases} 0, & k < k_{max}, \\ \pi, & k > k_{max}, \end{cases} \tag{57}$$

and

$$\lim_{\delta\to 0}|a_0|^2 = \frac{1}{|D|^2}\begin{vmatrix} d_0 & -\eta_1 V_{01} & -\eta_2 V_{02} & \cdots \\ d_1 & 1-\eta_1 V_{11} & -\eta_2 V_{12} & \cdots \\ d2 & -\eta_1 V_{21} & 1-\eta_2 V_{22} & \cdots \\ \vdots & \vdots & \vdots & \ddots \end{vmatrix} < \infty. \tag{58}$$

One can see the value of $|a_0|$ becomes finite for $\delta \to 0$. So we obtain $\lim_{\delta\to 0}\mathrm{Im}(\frac{1}{\eta_0})|a_0|^2 = 0$, namely, the first term on the right side of Eq. (55) vanishes. This means that the photoabsorption cross section of Eq. (55) is not divergent for any incident photon energy ω.

Dropping the first term on the right side of Eq. (55), and substituting Eq. (53) into the second term of Eq. (55), we obtain the absorption cross section

$$\sigma(\omega) = 4\pi^2\alpha\omega\sum_{k>k_{max}} c_k\frac{|P_k|^2}{|A|^2}\left\{\frac{(e + q_k)^2}{e^2 + 1} + d_L(k)\frac{\tilde{\Gamma}/(2\pi)}{(\omega - \varepsilon_r)^2 + (\tilde{\Gamma}/2)^2}\right\}, \tag{59}$$

where

$$q_k = \frac{1}{\lambda}\left[\mathrm{Re}\left(\frac{Q_k}{P_k}\right) - \gamma\right], \tag{60}$$

$$d_L(k) = \frac{\pi\tilde{\Gamma}}{2\lambda^2}\left[\mathrm{Im}\left(\frac{Q_k}{P_k}\right)\right]^2. \tag{61}$$

The photoabsorption cross section, Eq. (59), is the superposition of the "Fano profile" and "Lorentz profile," but the factors q_k and $\tilde{\Gamma}$ in these profiles depend slightly on the photon energy ω. At $\varepsilon = \varepsilon_r$, the factor q_k is considered as the q value of the Fano profile.

C. Numerical scheme to calculate the photoabsorption cross section

Here, we present the scheme for calculating the photoabsorption cross section of plasmas. We assume that $E_1, E_2, \ldots, E_N$ are electronic optical transition energies $\Delta\varepsilon$ of the AA which are calculated by eigenvalues of the LDA equation (1).

For calculating the photoabsorption cross section in the range $(0, \omega_{max})$ of photon energy, we divide this range into some small intervals as follows:

$$\begin{cases} 0 < \omega \le \frac{1}{2}(E_1 + E_2), \\ \frac{1}{2}(E_1 + E_2) < \omega \le \frac{1}{2}(E_2 + E_3), \\ \frac{1}{2}(E_2 + E_3) < \omega \le \frac{1}{2}(E_3 + E_4), \\ \vdots \\ \frac{1}{2}(E_{N-1} + E_N) < \omega \le \omega_{max}. \end{cases} \tag{62}$$

TABLE I. The energies, occupation numbers $f_{n\ell}$, and the charge state Z^* of the Fe ion in Fe plasma, and the chemical potential μ of Fe plasma obtained by our FTDFT and Grimaldi [24]. The plasma density and temperature are 7.85 g/cm^3 and 100 eV, respectively.

Orbital	$f_{n\ell}$		Energy [a.u.]	
	Present	Grimaldi	Present	Grimaldi
$1s$	1.00000	1.0000	−258.407	−258.14
$2s$	0.999280	0.9992	−33.3265	−32.942
$2p$	0.997906	0.9977	−29.3981	−29.008
$3s$	0.418225	0.4117	−5.52423	−5.4112
$3p$	0.340303	0.3345	−4.30461	−4.1947
$3d$	0.232670	0.2269	−2.35194	−2.2184
$4s$	-	0.1438	-	−0.16614
Z^*	(present)	10.8090		
	(Grimaldi)	10.697		
μ	(present)	−6.73719 [a.u.]		

In each small interval of photon energy, we calculate $\sigma(\omega)$ of Eq. (59) employing the wave functions obtained by Eq. (1). If the competition between successive excitation and direct photoionization does not occur in a given interval, the $\sigma(\omega)$ of Eq. (59) vanishes in that interval. In this case, we calculate the photoabsorption cross section by means of the following equation,

$$\sigma(\omega) = 4\pi^2 \alpha \omega \sum_{k>k_{max}} c_k |d_k|^2 P(\omega), \tag{63}$$

where $P(\omega)$ is the normalized Gaussian-type line profile with the Doppler width. The photoabsorption cross section, Eq. (63), is identical to the one in the case where electrons of an AA are responding independently to the external field.

III. RESULTS AND DISCUSSION

We have applied our theory to a Fe plasma ($T=100$ eV, $\rho_{ion}=8.465\times10^{22}$ cm^{-3}). Table I shows the atomic data obtained by our FTDFT calculations. This Fe plasma is in liquid range because the coupling constant $\Gamma_{coupling} \equiv Z^{*2}/(a_{ion}T)$ for this plasma is $\simeq 12$, so the HNC approximation may be suitable for this plasma [34,35].

The potential of Eq. (2) around a nucleus in Fe plasma is shown by "a" in Fig. 1. One can see that the potential becomes positive in the region of $r=a_{ion}$. The existence of the positive region in the potential is due to the charges of other ions and electrons surrounding the AA located at the origin. This positive region of the potential grows into a large hump when the plasma density is large or the plasma temperature is low and completely disappears when the plasma density is low or the plasma temperature is high. The onset of this hump coincides with the onset of growth of the first peak of the radial distribution function $g_{ii}(R)$, which is shown in Fig. 2. In a plasma where the potential of Eq. (2) has a positive region, no bound states with large principal quantum numbers can exist in the AA due to pressure ionization. Consequently, the number of orbitals of the AA is finite. In our calculation of the Fe plasma, the $4s$ state is not bound.

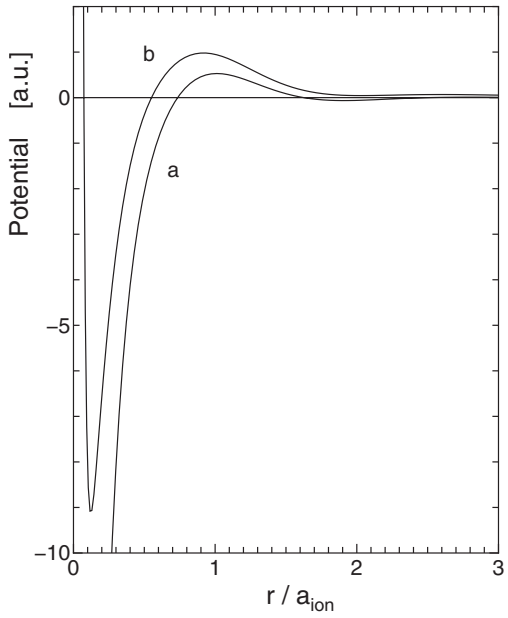

FIG. 1. The potentials. a: The potential $V(r)$ of Eq. (2) for an AA in the Fe plasma ($\rho_{ion}=7.85$ g/cm^3, $T=100$ eV) that has the positive region near the $r=a_{ion}$. b: The potential "a" with the centrifugal potential $\ell(\ell+1)/2r^2(\ell=2)$.

The calculated optically allowed transitions and their transition energies $\Delta\varepsilon$ for the Fe ion are shown in Table II. The absorption cross section for the photon energy in the range of 22–34 [a.u.] is shown in Fig. 3, where the three Fano profiles appear at the photon energies of 23 [a.u.], 27 [a.u.], and 29 [a.u.], respectively. The resonance energy positions of these Fano profiles are shifted from the positions of the transition energies. The shifts obtained by our scheme are con-

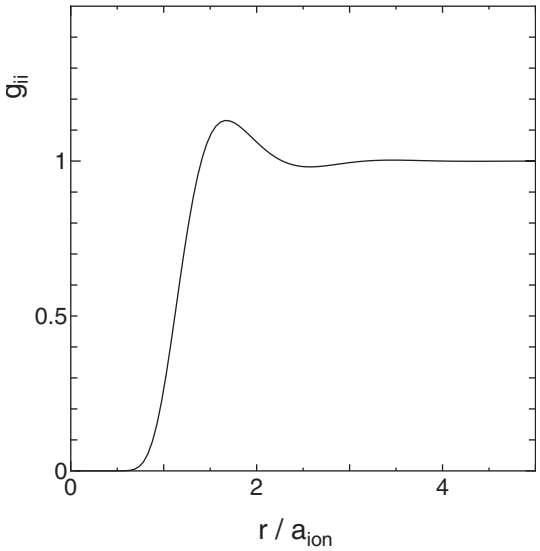

FIG. 2. The radial distribution function $g_{ii}(r)$ obtained from our FTDFT for the Fe plasma ($\rho_{ion}=7.85$ g/cm^3, $T=100$ eV). The coupling constant Γ of this Fe plasma is $\Gamma\simeq12$.

TABLE II. Transition energies $\Delta\varepsilon$ for the optically allowed transitions, these are the differences between two eigenvalues obtained by our FTDFT and Grimaldi [24] for the Fe plasma.

	$\Delta\varepsilon$ [a.u.]	
Transition	Present	Grimaldi
$3s \rightarrow 3p$	1.21962	1.216
$3p \rightarrow 3d$	1.95266	1.976
$2s \rightarrow 2p$	3.92837	3.933
$3p \rightarrow 4s$	-	4.029
$2p \rightarrow 3s$	23.8739	23.59
$2p \rightarrow 3d$	27.0462	26.79
$2s \rightarrow 3p$	29.0219	28.75
$2p \rightarrow 4s$	-	28.84

siderably larger than Grimaldi's results, which include line shifts and linewidths obtained from the level self-energies. In Table III, we show the differences between resonance energy position and transition energy $\Delta\varepsilon$, resonance widths $\tilde{\Gamma}$, and q values which are obtained by our scheme.

The Fano profile at energy of 27 [a.u.] is explained as a result of the two competing transitions of $2p \rightarrow 3d$ and $3d \rightarrow \varepsilon(\ell=1 \text{ or } 3)$. In Fig. 4, we show the profile in the vicinity of the peak of this Fano profile. From this figure, our calculation shows that the line profile does not diverge and its peak value is finite.

The structure at photon energy 29.6 [a.u.] is not the Fano profile but the edge profile in the vicinity of the threshold of $2p$. The electron ejected from the $2p$ shell with an angular momentum $\ell=0$ moves in the potential shown by "a" in Fig. 1. From this figure, it is clear that there exists a large amount of the wave function for this electron inside of the ion sphere radius. So, the overlap between the wave function of the ejected electron and the one of the $2p$ shell becomes large, therefore, the transition probability is enhanced. In Fig. 5, we show the edge profile in the region of this $2p$ threshold, where the broken line shows the profile of the transition $2p \rightarrow \varepsilon(\ell=0)$ only, the light solid line shows the cross section without the transition $2p \rightarrow \varepsilon(\ell=0)$, and the heavy solid line shows the total cross section.

In Fig. 6, we show the photoabsorption cross section in the energy range $0 \sim 6$ [a.u.]. A narrow Fano profile due to the $2s \rightarrow 2p$ appears in this figure at resonance energy position of the photon energy of 3.93 [a.u.]. Though it seems there are another two resonances due to $3s \rightarrow 3p$ and $3p \rightarrow 3d$ in this figure, these resonances cannot occur because the transition energy of $|\varepsilon_{3p}-\varepsilon_{3s}|$ (or $|\varepsilon_{3d}-\varepsilon_{3p}|$) is less than the ionization energy of the $3p$ (or the $3d$) electrons. Instead, the usual bound-bound transitions by photoabsorption without relaxation occur. In Fig. 6, we show the two usual bound-bound absorption lines for the $3s$-$3p$ and $3p$-$3d$ transitions with the Doppler width. These are obtained with Eq. (63),

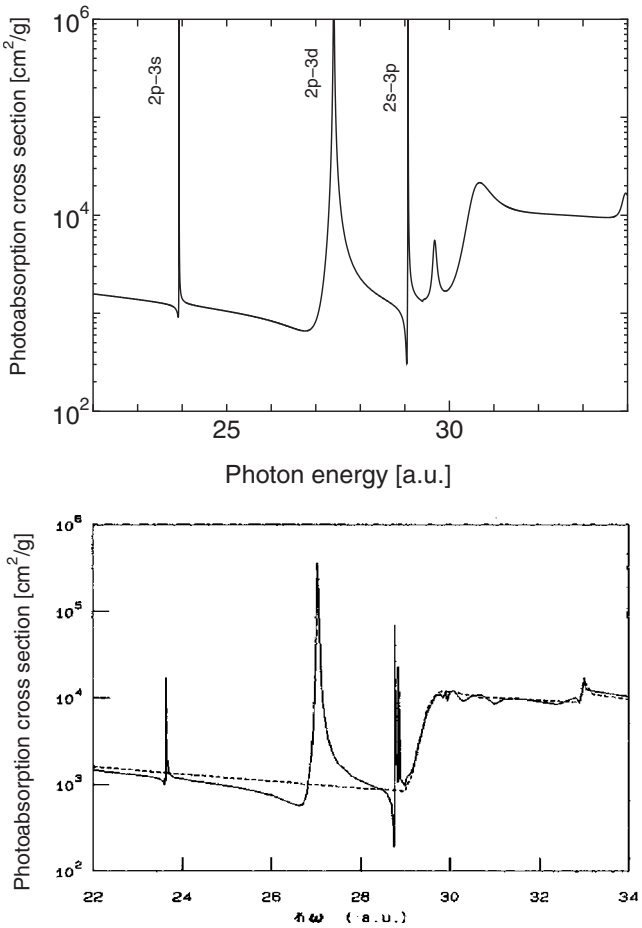

FIG. 3. The photoabsorption cross section of Fe plasma ($\rho_{ion}=7.85$ g/cm^3, $T=100$ eV). Upper panel; our scheme, lower panel, Grimaldi *et al.* transcribed from Ref. [24].

TABLE III. The parameters of the Fano profiles, $\varepsilon_r-\Delta\varepsilon$ [a.u.], $\tilde{\Gamma}$ [a.u.], and q, which are obtained by our scheme. $\Delta\varepsilon$ is the energy given in Table II. The line profile obtained at resonance energy position is composed by the Fano profile and the Lorentz profile. The peak values of the Fano and the Lorentz profiles are proportional to the q_k^2+1 and $d_L(k)$, respectively, so that, as shown in this table, the Lorentz profile is a negligible amount.

Resonance	$\varepsilon_r-\Delta\varepsilon$ [a.u.]	$\tilde{\Gamma}$	q_k	q_k^2	$d_L(k)$
$2p \rightarrow 3s(\varepsilon p)$	0.057	2.16694×10^{-4}	1.29909×10^{2}	1.68762×10^{4}	5.59501×10^{-1}
$2p \rightarrow 3d(\varepsilon p)$	0.358	1.50620×10^{-2}	-1.18565×10^{2}	1.40576×10^{4}	6.68707×10^{0}
$2p \rightarrow 3d(\varepsilon f)$	0.358	1.50620×10^{-2}	1.08855×10^{2}	1.18495×10^{4}	6.6269×10^{-3}
$2s \rightarrow 3p(\varepsilon s)$	0.051	4.42277×10^{-4}	2.92585×10^{2}	8.56060×10^{4}	1.01332×10^{0}
$2s \rightarrow 3p(\varepsilon d)$	0.051	4.42277×10^{-4}	5.26407×10^{1}	2.77105×10^{3}	1.00126×10^{-1}

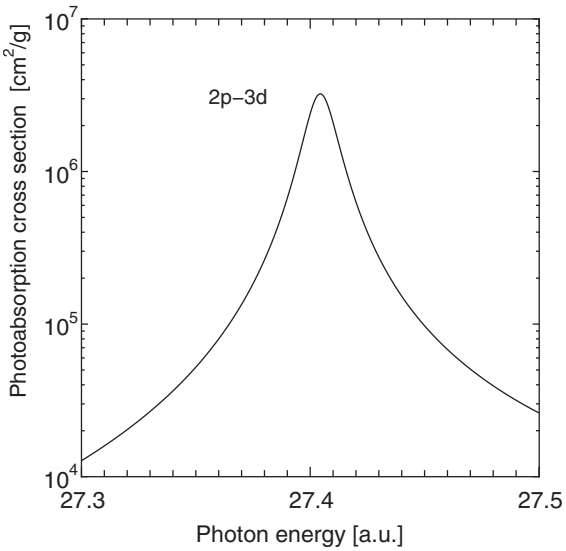

FIG. 4. Closeup of the line profile obtained in the vicinity of the peak for the resonance $2p \rightarrow 3d$ shown in Fig. 3.

the independent-particle model in the calculation of the transition probability. The absorption cross sections shown in Fig. 3 and Fig. 6 are in reasonable agreement with that of Grimaldi [24], indicating that the dropped terms of Eq. (23) make negligible contributions to the absorption cross section.

IV. CONCLUSION

We have given a derivation of the Fano profile (the resonance energy position, the resonance width Γ, and q value) from the TDDFT, and have proposed a scheme for calculating the photoabsorption cross section with relaxation of the system. We have shown that our scheme is applicable to the calculation of photoabsorption of LTE plasmas.

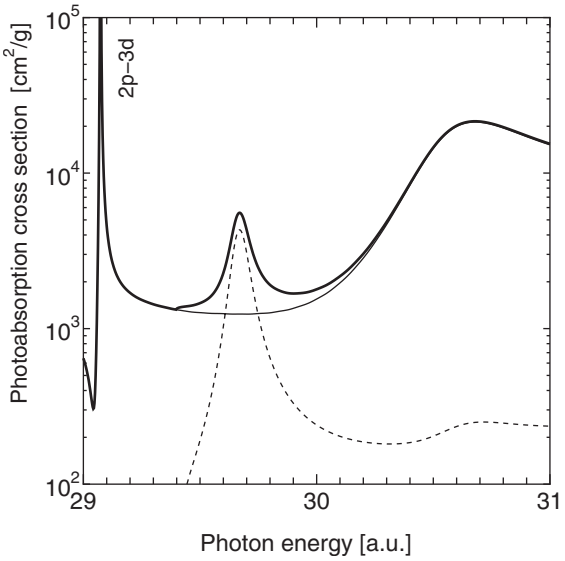

FIG. 5. Comparison of the total photoabsorption cross section (heavy solid line) shown in Fig. 3 and the cross section without a transition $2p \rightarrow \varepsilon(\ell=0)$ (light solid line). The cross section for the only $2p \rightarrow \varepsilon(\ell=0)$ transition is also shown (dashed line).

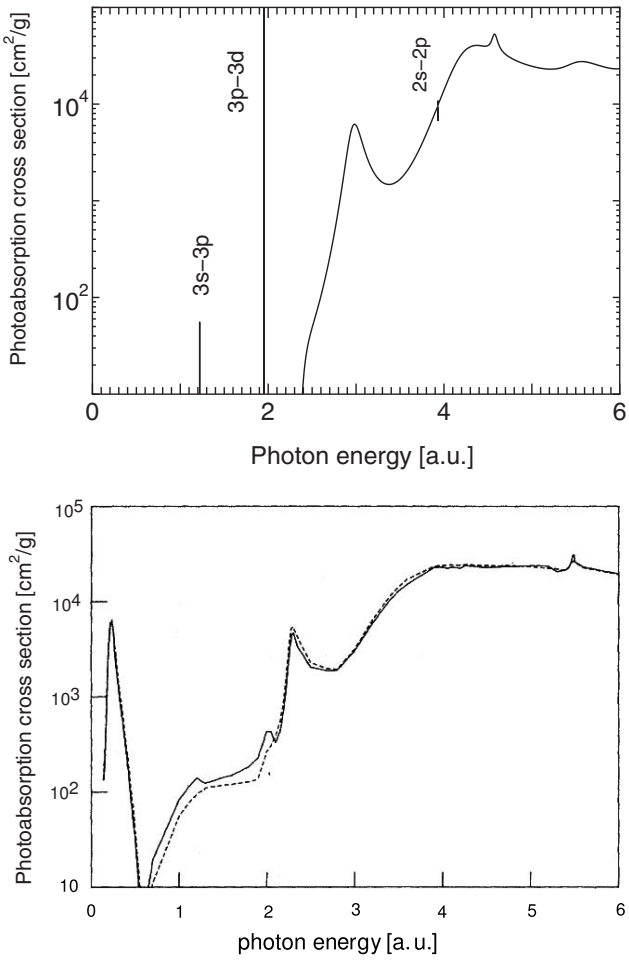

FIG. 6. The photoabsorption cross section of the Fe plasma in the range of the photon energy less than 6 [a.u.]. (ρ_{ion} = 7.85 g/cm^3, T = 100 eV). Upper panel, our scheme; the lines $3s-3p$ and $3p-3d$ are calculated by Eq. (60). Lower panel, Grimaldi *et al.*, transcribed from Ref. [24].

This scheme has made clear that the line profile in the vicinity of the resonance energy position is composed of the Fano profile and the Lorentz profile, an that these profiles do not appear when the bound-bound transition and the bound-free transition do not compete.

The photoabsorption cross sections of Fe plasma (T = 100 eV, $\rho_{ion} = 8.465 \times 10^{22}$ cm^{-3}) have been calculated by our scheme, and it has been shown that the results of the cross sections are in good agreement with those of Grimaldi. Thus, we conclude that the dropped terms of Eq. (23) make negligible contribution to the absorption cross section for plasmas.

ACKNOWLEDGMENTS

We acknowledge fruitful discussions on the subject of DFT with J. Chihara of Japan Atomic Energy Agency and G. Faussurier of CEA/DAM Ile-de-France, and we thank T. Kagawa of Nara Women's University for the careful reading of the manuscript.

APPENDIX A: REWRITING THE DOUBLE SUM TO A SINGLE SUM

For example, we assume that all bound states of the AA obtained are $1s$, $2s$, $2p$, and $3s$, and the incident photon energy ω is in the vicinity of the difference between ε_{2p} and ε_{3s}. Then, the first and the second terms of Eq. (29) are written as follows:

$$\begin{aligned}
&2[f(\varepsilon_{n_i\ell_i}) - f(\varepsilon_{n_f\ell_f})]C_{\ell_i\ell_f}\eta_{n_i\ell_i,n_f\ell_f}R_{n_i\ell_i}(r)R_{n_f\ell_f}(r)R_{n_f\ell_f}(r')R_{n_i\ell_i}(r') \\
&\quad + \sum_{\varepsilon_{n\ell}<\varepsilon_{n'\ell'}} 2[f(\varepsilon_{n\ell}) - f(\varepsilon_{n'\ell'})]C_{\ell\ell'}\eta_{n\ell,n'\ell'}R_{n\ell}(r)R_{n'\ell'}(r)R_{n'\ell'}(r')R_{n\ell}(r') \\
&\quad = 2[f(\varepsilon_{2p}) - f(\varepsilon_{3s})]C_{10}\eta_{2p,3s}R_{2p}(r)R_{3s}(r)R_{3s}(r')R_{2p}(r') + 2[f(\varepsilon_{1s}) - f(\varepsilon_{2p})]C_{01}\eta_{1s,2p}R_{1s}(r)R_{2p}(r)R_{2p}(r')R_{1s}(r') \\
&\quad\quad + 2[f(\varepsilon_{2s}) - f(\varepsilon_{2p})]C_{01}\eta_{2s,2p}R_{2s}(r)R_{2p}(r)R_{2p}(r')R_{2s}(r'). \qquad \text{(A1)}
\end{aligned}$$

These three terms are numbered 0 to 2 ($k_{max}=2$) as shown in following table:

$(n\ell, n'\ell')$	$(1s,2p)$	$(2s,2p)$	$(2p,3s)$
k	1	2	0

Then, we can rewrite the right side of Eq. (A1) to a sum,

$$\sum_{k=0}^{2} c_k\eta_k U_k(r)U_k(r'), \qquad \text{(A2)}$$

where factors c_k, η_k and function $U_k(r)$ are

$$k=0:\begin{cases} c_0 = 2[f(\varepsilon_{2p}) - f(\varepsilon_{3s})]C_{10}, \\ \eta_0 = \eta_{2p,3s}, \\ U_0(r) = R_{2p}(r)R_{3s}(r), \end{cases} \qquad \text{(A3)}$$

$$k=1:\begin{cases} c_1 = 2[f(\varepsilon_{1s}) - f(\varepsilon_{2p})]C_{01}, \\ \eta_1 = \eta_{1s,2p}, \\ U_1(r) = R_{1s}(r)R_{2p}(r), \end{cases} \qquad \text{(A4)}$$

$$k=2:\begin{cases} c_2 = 2[f(\varepsilon_{2s}) - f(\varepsilon_{2p})]C_{01}, \\ \eta_2 = \eta_{2s,2p}, \\ U_2(r) = R_{2s}(r)R_{2p}(r). \end{cases} \qquad \text{(A5)}$$

The third term of Eq. (29) is written as

$$\begin{aligned}
&-i\pi\sum_{n\ell\ell'} 2[f(\varepsilon_{n\ell}) \\
&\quad - f(E_f)]C_{\ell\ell'}R_{nl}(r)R_{E_f\ell'}(r)R_{E_f\ell'}(r')R_{n\ell}(r')\theta(E_f) \\
&\quad = -i\pi 2[f(\varepsilon_{1s}) - f(\varepsilon_{1s} \\
&\quad + \omega)]C_{01}R_{1s}(r)R_{(\varepsilon_{1s}+\omega)p}(r)R_{(\varepsilon_{1s}+\omega)p}(r')R_{1s}(r')\theta(\varepsilon_{1s}+\omega) \\
&\quad\quad - i\pi 2[f(\varepsilon_{2s}) - f(\varepsilon_{2s} \\
&\quad + \omega)]C_{01}R_{2s}(r)R_{(\varepsilon_{2s}+\omega)p}(r)R_{(\varepsilon_{2s}+\omega)p}(r')R_{2s}(r')\theta(\varepsilon_{2s}+\omega) \\
&\quad\quad - i\pi 2[f(\varepsilon_{2p}) - f(\varepsilon_{2p} \\
&\quad + \omega)]C_{10}R_{2p}(r)R_{(\varepsilon_{2p}+\omega)s}(r)R_{(\varepsilon_{2p}+\omega)s}(r')R_{2p}(r')\theta(\varepsilon_{2p}+\omega) \\
&\quad\quad - i\pi 2[f(\varepsilon_{2p}) - f(\varepsilon_{2p} \\
&\quad + \omega)]C_{12}R_{2p}(r)R_{(\varepsilon_{2p}+\omega)d}(r)R_{(\varepsilon_{2p}+\omega)d}(r')R_{2p}(r')\theta(\varepsilon_{2p}+\omega) \\
&\quad\quad - i\pi 2[f(\varepsilon_{3s}) - f(\varepsilon_{3s} \\
&\quad + \omega)]C_{01}R_{3s}(r)R_{(\varepsilon_{3s}+\omega)p}(r)R_{(\varepsilon_{3s}+\omega)p}(r')R_{3s}(r')\theta(\varepsilon_{3s}+\omega). \qquad \text{(A6)}
\end{aligned}$$

All terms on the right side of Eq. (A6) are numbered 3, $4,\ldots,7$ as shown in following table:

$(n\ell, \ell')$	$(1s,p)$	$(2s,p)$	$(2p,s)$	$(2p,d)$	$(3s,p)$
k	3	4	5	6	7

and we rewrite the right side of Eq. (A6) as

$$\sum_{k=3}^{7} c_k\eta_k U_k(r)U_k(r'). \qquad \text{(A7)}$$

For example, some factors in this sum are shown as

$$k=3:\begin{cases} c_3 = 2[f(\varepsilon_{1s}) - f(\varepsilon_{1s}+\omega)]C_{01}\theta(\varepsilon_{1s}+\omega), \\ \eta_3 = -i\pi, \\ U_3(r) = R_{1s}(r)R_{(\varepsilon_{1s}+\omega)p}(r), \end{cases} \qquad \text{(A8)}$$

$$k=4:\begin{cases} c_4 = 2[f(\varepsilon_{2s}) - f(\varepsilon_{2s}+\omega)]C_{01}\theta(\varepsilon_{2s}+\omega), \\ \eta_4 = -i\pi, \\ U_4(r) = R_{2s}(r)R_{(\varepsilon_{2s}+\omega)p}(r), \end{cases} \qquad \text{(A9)}$$

$$k=5:\begin{cases} c_5 = 2[f(\varepsilon_{2p}) - f(\varepsilon_{2p}+\omega)]C_{10}\theta(\varepsilon_{2p}+\omega), \\ \eta_5 = -i\pi, \\ U_5(r) = R_{2p}(r)R_{(\varepsilon_{2p}+\omega)s}(r). \end{cases} \qquad \text{(A10)}$$

Then, Eq. (29) is rewritten as

$$\begin{aligned}
\chi^0_\omega(r,r') &= \sum_{k=0}^{2} c_k\eta_k U_k(r)U_k(r') + \sum_{k>2} c_k\eta_k U_k(r)U_k(r') \\
&= \sum_{k=0}^{7} c_k\eta_k U_k(r)U_k(r'). \qquad \text{(A11)}
\end{aligned}$$

APPENDIX B: EXCHANGE-CORRELATION POTENTIAL

The exchange-correlation potential at finite temperature employed in our FTDFT is given as follows [32]:

$$v_{xc}[\rho] = \mu_x(r_s,t) + \mu_c(r_s,t), \tag{B1}$$

where ρ is an electron density and r_s is the electron sphere radius (hereafter atomic units),

$$r_s = \left(\frac{3}{4\pi\rho}\right)^{1/3},$$

and t is ratio of electron temperature T to the zero-temperature Fermi energy $E_f = \frac{1}{2}(3\pi^2\rho)^{2/3}$,

$$t = \frac{T}{E_f}.$$

The functions $\mu_x(r_s,t)$ and $\mu_c(r_s,t)$ in Eq. (B1) are given as

$$\mu_x(r_s,t) = -\left(\frac{9}{4\pi^2}\right)^{1/3}\frac{1}{r_s} \times\left(\frac{1 + 2.834\,31t^2 - 0.215\,12t^2 + 5.275\,86t^4}{1 + 3.943\,09t^2 + 7.913\,79t^4} \times\tanh(1/t)\right), \tag{B2}$$

$$\mu_c(r_s,t) = -0.02545\ln(1 + 19/r_s)(1 + c_1 t + c_2 t^{1/4})e^{-c_3 t} - 0.638\,168\sqrt{\frac{t}{r_s}}\tanh(1/t)e^{-c_4/t}. \tag{B3}$$

The factors c_1, c_2, c_3, and c_4 in $\mu_c(r_s,t)$ are given as

$$\begin{cases} c_1 = \dfrac{9.554\,32}{1 + 0.066\,66r_s}, \\ c_2 = \dfrac{3.579\,12 - 5.990\,65r_s^{1/4} + 1.297\,22r_s^{3/4}}{1 + 1.611\,26r_s^{1/4}}, \\ c_3 = \dfrac{4.802\,17}{1 + 0.423\,387\sqrt{r_s}}, \\ c_4 = 0.293\,35 + 0.322\,565\sqrt{r_s}. \end{cases}$$

In original paper [32], the exponential function on the first term of the right-hand side of Eq. (B3) is expressed as $e^{-c_3/t}$, but the author of the present paper thinks this expression may be a typing error.

[1] D. S. J. Stein and A. Ron, Phys. Rev. A **31**, 446 (1985).
[2] W. R. Johnson, C. Guet, and G. F. Bertsch, J. Quant. Spectrosc. Radiat. Transf. **99**, 327 (2006).
[3] B. F. Rozsnyai, Phys. Rev. E **55**, 7507 (1997).
[4] A. G. T. Blenski and F. Perrot, Phys. Rev. E **55**, R4889 (1997).
[5] M. W. C. Dharma-wardana and F. Perrot, Phys. Rev. A **26**, 2096 (1982).
[6] J. Chihara, Prog. Theor. Phys. **59**, 76 (1978).
[7] F. Perrot, Phys. Rev. E **47**, 570 (1993).
[8] C. Blancard and G. Faussurier, Phys. Rev. E **69**, 016409 (2004).
[9] A. Bar-Shalom, J. Oreg, and M. Klapisch, J. Quant. Spectrosc. Radiat. Transf. **99**, 35 (2006).
[10] M. W. C. Dharma-wardana, Phys. Rev. E **73**, 036401 (2006).
[11] B. F. Rozsnyai, Phys. Rev. A **43**, 3035 (1991).
[12] J. Zeng, F. Jin, J. Yuan, and Q. Lu, Phys. Rev. E **62**, 7251 (2000).
[13] J. C. Pain and T. Blenski, J. Quant. Spectrosc. Radiat. Transf. **81**, 355 (2003).
[14] A. Bar-Shalom, J. Oreg, W. H. Goldstein, D. Shvarts, and A. Zigler, Phys. Rev. A **40**, 3183 (1989).
[15] T. Blenski and K. Ishikawa, Phys. Rev. E **51**, 1602 (1995).
[16] A. Zangwill and P. Soven, Phys. Rev. A **21**, 1561 (1980).
[17] M. J. Scott and E. Zaremba, Phys. Rev. A **21**, 12 (1980).
[18] V. L. Jacobs, E. Bechar, and B. F. Rozsnyai, J. Quant. Spectrosc. Radiat. Transf. **71**, 397 (2001).
[19] X. Tong and S. Chu, Phys. Rev. A **55**, 3406 (1997).
[20] M. Stener, G. DeAlti, G. Fronzoni, and P. Decleva, Chem. Phys. **222**, 197 (1997).
[21] E. K. U. Gross and W. Kohn, Phys. Rev. Lett. **55**, 2850 (1985).
[22] S. Erkoc and H. J. F. Jansen, Phys. Rev. A **59**, 2490 (1999).
[23] T. Blenski, J. Quant. Spectrosc. Radiat. Transf. **99**, 84 (2006).
[24] F. Grimaldi *et al.*, Phys. Rev. A **32**, 1063 (1985).
[25] A. Neogi *et al.*, Phys. Rev. A **67**, 042707 (2003).
[26] P. Gauthier and S. J. Rose, Phys. Rev. E **58**, 942 (1998).
[27] S. Kiyokawa, J. Phys. Soc. Jpn. **64**, 4708 (1995).
[28] B. F. Rozsnyai, Phys. Rev. A **5**, 1137 (1972).
[29] D. A. Liberman, Phys. Rev. B **20**, 4981 (1979).
[30] J. C. Pain, G. Dejonghe, and T. Blenski, J. Quant. Spectrosc. Radiat. Transf. **99**, 451 (2006).
[31] B. Wilson, V. Sonnad, P. Sterne, and W. Isaacs, J. Quant. Spectrosc. Radiat. Transf. **99**, 658 (2006).
[32] F. Perrot and M. W. C. Dharma-wardana, Phys. Rev. A **30**, 2619 (1984).
[33] T. Blenski and B. Cichocki, J. Quant. Spectrosc. Radiat. Transf. **51**, 49 (1994).
[34] J. F. Springer, M. A. Pokrant, and J. F. A. Stevens, J. Chem. Phys. **58**, 4863 (1973).
[35] K.-C. Ng, J. Chem. Phys. **61**, 2680 (1974).